Component Dynamics in Miscible Blends of 1,4-Polyisoprene and 1,2-Polybutadiene

Jeffrey A. Zawada† **and Gerald G. Fuller***

Department of Chemical Engineering, Stanford University, Stanford, California 94305-5025

Ralph H. Colby

Imaging Research and Advanced Development, Eastman Kodak Company, Rochester, New York 14650-2109

Lewis J. Fetters

Corporate Research—Science Laboratories, Exxon Research and Engineering Company, Annandale, New Jersey 08801

Jacques Roovers

Institute for Environmental Chemistry, National Research Council of Canada, Ottawa, Ontario, Canada K1A 0R6

Received October 22, 1993; Revised Manuscript Received August 5, 1994®

ABSTRACT: The effects of blending on the rheology of the individual components in highly entangled miscible blends of 1,4-polyisoprene (PI) and 1,2-polybutadiene (1,2-PB) are investigated. Blend component contributions to the dynamic modulus, $G^*(\omega)$, are recovered over the full composition range by complementing dynamic mechanical rheometry with infrared polarimetry. Distinct relaxations for each component are observed. Analysis of the modulus amplitudes of the component $G^*(\omega)$ contributions reveals that the behavior of the slower relaxing component, 1,2-PB, compares well with constraint release scaling predictions. Each component is found to have a different average number of skeletal bonds between entanglements, in agreement with the predictions of an existing entanglement theory. The components appear to adopt a single reptation tube diameter and a mutual modulus shift factor, $b_T(T)$, in each blend. Analysis of the frequency dependence of the component $G^*(\omega)$ contributions indicates that each component's relaxation is governed by a distinct apparent glass transition temperature, T_g, and that at a constant $T - T_g$ blend composition only mildly influences the component relaxation times. A mild increase in the 1,2-PB relaxation time in the blend suggests a possible increase in the 1,2-PB friction factor in the presence of PI.

1.0. Introduction

The dynamics of miscible blends of chemically distinct polymers are significantly more complex than those of pure, monodisperse polymer melts, making the prediction of miscible blend rheology difficult. Successful models for highly entangled, monodisperse homopolymers, such as reptation theory,[1] fail dramatically when applied to miscible blends, reflecting that the dynamics of the blend components change upon blending. Thus, a critical step toward unraveling the complexity of the bulk blend behavior is understanding how the rheology of each component is influenced by the presence of the second species. Addressing this problem is not a simple matter, given that there are numerous interrelated means by which blending can potentially affect the component flow behaviors. In essence, each component brings to the blend a separate dynamic behavior, governed by distinct material properties, principally the monomeric friction factor, ζ_0, and the entanglement molecular weight, M_e. Changes in the local physical environment due to blending may effect changes in the component dynamics by directly altering these parameters or more subtly by influencing fundamental properties, such as the glass transition temperature, density, thermal expansion coefficient, fractional free volume, and chain dimensions, which influence ζ_0 and M_e. Any specific interactions between the dissimilar chains might induce additional variation in any of these parameters and thus alter the component dynamics. Still further modification of component dynamics may arise due to additional modes of relaxation, such as constraint release, that become available in the presence of a species with a faster relaxation rate.

Experimental progress in this field has been limited, largely because conventional rheometric techniques are capable of monitoring only bulk behavior and cannot isolate individual component contributions. In the preceding paper a method for separating the dynamic modulus $G^*(\omega)$ of a miscible blend into component contributions was developed based on complementing mechanical stress rheometry with infrared polarimetry measurements.[2] The obvious advantage of this method is that it provides a means of clearly monitoring the effects of blending on the rheology of each component. In this paper the method is applied to miscible blends of narrow molecular weight distribution 1,4-polyisoprene (PI) and atactic 1,2-polybutadiene (1,2-PB), and the effects of blend composition on the component contributions to G^* are closely examined.

Blends of PI and 1,2-PB serve as an attractive model system from an experimental standpoint since these species are miscible at all blend ratios. Homogeneity in blends of polyisoprene and 1,2-polybutadiene has been demonstrated by DSC[3,4] and TEM,[3] and true thermodynamic miscibility has been confirmed by ^{1}H NMR,[5] SANS,[6] and peel adhesion measurements of interdiffusion.[3] Moreover, blends of these hydrocarbons do not exhibit appreciable enthalpic interactions, as Roland demonstrated using FTIR.[7] Thus, PI/1,2-PB blends permit much of the richness of miscible blend rheology to be explored without

* To whom correspondence should be addressed.
† Present address: Eastman Chemical Co., Kingsport, TN 37662.
® Abstract published in *Advance ACS Abstracts*, September 15, 1994.

0024-9297/94/2227-6861$04.50/0

the introduction of additional complexity arising from strong intermolecular interactions. The absence of strong enthalpic interactions in these nearly ideal mixtures is reflected by the extremely small values of χ reported for this system. Trask and Roland[6] deduced from the observation of miscibility in a high molecular weight blend that χ must be less than 1.7×10^{-4}. More recently, using SANS Tomlin and Roland[8] found χ to actually be negative and have a magnitude on the order of 10^{-3}. For blends containing 1,2-PB of lower vinyl content (which are known to be less miscible, as they have a lower critical solution temperature[9,10]) SANS results[11,12] give a positive χ on the order of 10^{-3} (or less) for high molecular weight blends. In the absence of interchain attractions, molecular compatibility for these polymers is made possible by the near equivalence of van der Waals dispersive energy densities and near equivalence of liquid structure (free volume).[6,7] As a result, the small combinatorial entropy of mixing is sufficient to drive miscibility.

Additional advantages of the PI/1,2-PB system include low glass transition temperatures, alleviating the need to conduct experiments at highly elevated temperatures, and disparate component stress-optic coefficients, facilitating distinction of component contributions to birefringence.

2.0. Experimental Section

The blends used in this study are the same as those used in the previous paper to demonstrate the feasibility of the G^* separation technique and to assess orientational coupling.[2] Blends containing 20, 40, 60, and 80% 1,2-PB by weight were prepared from narrow molecular weight distribution 1,4-polyisoprene (76% 1,4-*cis*; M_w = 75 000) and 1,2-polybutadiene (M_w = 204 000). All blends contain 6% by weight perdeuterated polyisoprene (77% 1,4-*cis*; M_w = 90 000), having nearly the same degree of polymerization as the undeuterated PI, to facilitate the IR dichroism measurements discussed in the previous report. All three components have $M_w/M_n < 1.1$, and the 1,2-PB has a microstructure with >99% 1,2-units. Further details regarding the pure component characteristics, including microstructures, and blend preparation may be found in ref 2.

Glass transitions of the pure components and the blends were measured using a DuPont 910 differential scanning calorimeter. The glass transition temperature, T_g, was recovered from the midpoint of the heat capacity transition in an upward temperature scan at 10 °C/min using 7–14 mg samples. Reproducibility was verified by repeating all measurements at least once.

Mechanical oscillatory shear rheometry was conducted to measure the blend dynamic modulus at temperatures well above T_g using a Rheometrics RMS-800 rheometer with parallel plate geometry (8 mm diameter plates, 1–2 mm gap heights). Strain frequencies ranging from 0.01 to 100 rad/s were studied, and the sample temperature was controlled by circulating heated nitrogen through the sample chamber.

Oscillatory shear IR dichroism and birefringence measurements were conducted using a previously described apparatus[13,14] with several modifications.[2] Parallel plate shear geometry was used. The frequencies used in the optical experiments spanned from as low as 0.01 to 100 rad/s, and strain amplitudes ranged from 0.15 to 0.30 on 0.5 mm thick samples, where the higher strains were applied at the lower frequencies. Linear viscoelasticity was verified by consistent results at strains ranging from 0.10 to 0.50. Experiments were conducted at 21, 40, 60, 80, and 100 °C (except for pure PI, for which experiments were run at 21, 30, 40, and 50 °C due to its fast relaxation). Experiments for each set of conditions were repeated at least once to ensure reproducibility. IR dichroism measurements were made to verify that the component stress-optic coefficients (for birefringence) are not composition dependent. Validity of this assumption for the PI/1,2-PB blend system was demonstrated previously,[2] and so here we need only consider the birefringence measurements.

3.0. Recovery of Component $G^*(\omega)$ Contributions

In this section highlights of the method for identifying the component contributions to the blend dynamic modulus are described. For a more complete development of the analysis technique, the interested reader is referred to ref 2. In both the mechanical and optical experiments small-amplitude sinusoidal shear strains are applied, having a maximum amplitude γ° and frequency ω (i.e., $\gamma(t) = \gamma^\circ \sin \omega t$). Shear is applied in the 1-direction and the velocity gradient is along the 2-axis. Within the limit of linear viscoelasticity the shear stress, σ_{12}, and the normal stress differences, $N_1 = \sigma_{11} - \sigma_{22}$, $N_2 = \sigma_{22} - \sigma_{33}$, and $N_3 = N_1 + N_2$, experienced by the material have responses which can be concisely expressed in terms of the strain variables and the viscoelastic material functions G', G'', ψ_j', ψ_j'', and ψ_j^d:[15]

$$\sigma_{12}(t) = \gamma^\circ[G'(\omega) \sin \omega t + G''(\omega) \cos \omega t] \quad (1)$$

$$N_j(t) = (\gamma^\circ\omega)^2[\psi_j^d(\omega) + \psi_j'(\omega) \cos 2\omega t + \psi_j''(\omega) \sin 2\omega t] \quad (2)$$

where $j = 1, 2, 3$. The complex dynamic modulus is $G^*(\omega) = G'(\omega) + iG''(\omega)$, the complex normal stress difference coefficients are $\psi_j^*(\omega) = \psi_j'(\omega) - i\psi_j''(\omega)$, and the normal stress difference displacement coefficients are $\psi_j^d(\omega)$. Dynamic mechanical rheometry provides $G^*(\omega)$ for the bulk, while the optical measurements are related to the component contributions to $\psi_3^*(\omega)$ and $\psi_3^d(\omega)$ for the choice of geometry used in the optical experiments. The 1,3-birefringence measured in these experiments can be written as

$$\Delta n'(t) = (\gamma^\circ\omega)^2[\psi_{3,Bi}^d(\omega) + \psi_{3,Bi}'(\omega) \cos 2\omega t + \psi_{3,Bi}''(\omega) \sin 2\omega t] \quad (3)$$

For the current purpose, we focus only on $\psi_{3,Bi}'$ and $\psi_{3,Bi}''$.

Since we are principally interested in the dynamic modulus rather than the third normal stress difference coefficients, expressions relating the material functions are necessary. Using well-established viscoelastic constitutive equations, $\psi_{3,Bi}'$ and $\psi_{3,Bi}''$ may be related to the optical analogs of G' and G'', as discussed in ref 2:

$$G_{Bi}'(\omega) = -\sum_{m=0}^{\infty} \frac{1}{2^m}[(2^m\omega)^2\psi_{3,Bi}'(2^m\omega)] \quad (4)$$

$$G_{Bi}''(\omega) = \sum_{m=0}^{\infty} \frac{1}{2^m}[(2^m\omega)^2\psi_{3,Bi}''(2^m\omega)] \quad (5)$$

These optical G^* coefficients are directly proportional to the true dynamic modulus, associated with the state of stress, due to the fact that σ_{ij} and n_{ij}' are fundamentally related to the orientation distribution of the polymer segments. For a melt of a single polymer species, the stress-optic rule provides a direct relationship between the optical and true dynamic modulus:

$$G_{Bi}^* = cG^* \quad (6)$$

where c is a material-dependent constant that can be assessed for the pure polymers from the ratio of G_{Bi}^* to G^*.

In miscible blends we assume the total stress is equal to the sum of the stress borne by each of the components. Thus, the mechanically acquired dynamic modulus for a blend of PI and 1,2-PB can be written as

$$G^* = G_{PI}^* + G_{PB}^* \quad (7)$$

Neglecting possible orientational coupling effects, which

contribute to birefringence but not to the state of stress, G_{Bi}^* is

$$G_{Bi}^* = c_{PI}G_{PI}^* + c_{PB}G_{PB}^* \quad (8)$$

where for the PI/1,2-PB system c_{PI} and c_{PB} were found to be composition independent and can thus be determined from the pure polymers.

For this blend system it was found that appreciable orientational coupling between chain segments does arise and can be sufficiently characterized by a single coupling coefficient[2] $\epsilon = 0.35 \pm 0.05$. Incorporating orientational coupling into the analysis of the birefringence by Doi and co-workers[16] leads to the following expression[2] for G_{Bi}^*:

$$G_{Bi}^* = c_{PI}(1-\epsilon)\left[\frac{G_{PI}^* + \frac{\phi_{PI}}{\phi_{PB}}\left(\frac{\phi_{PB}\epsilon}{1-\phi_{PB}\epsilon}\right)G_{PB}^*}{(1-\phi_{PI}\epsilon) - \left(\frac{\phi_{PB}\epsilon}{1-\phi_{PB}\epsilon}\right)\phi_{PI}\epsilon}\right] + c_{PB}(1-\epsilon)\left[\frac{G_{PB}^* + \frac{\phi_{PB}}{\phi_{PI}}\left(\frac{\phi_{PI}\epsilon}{1-\phi_{PI}\epsilon}\right)G_{PI}^*}{(1-\phi_{PB}\epsilon) - \left(\frac{\phi_{PI}\epsilon}{1-\phi_{PI}\epsilon}\right)\phi_{PB}\epsilon}\right] \quad (9)$$

where ϕ_i is the volume fraction of component i. Equations 7 and 9 can easily be solved for the desired component contributions G_{PI}^* and G_{PB}^*.

4.0. Pure Component Dynamics

The empirical time–temperature superposition principle[15] was used to generate the master curves for the pure component G^* and G_{Bi}^* shown in Figure 1 on scales appropriate for comparing the mechanical and optical results. The frequency shift factor a_T and modulus shift factor b_T are defined by the relationship $G^*(\omega;T) = b_T G^*(a_T\omega;T_0)$. Values for a_T, b_T, and stress-optic coefficients c (calculated from the ratio of G_{Bi}^* to G^*) are listed in Table 1. Actually, c is the product of the stress-optic coefficient and a constant factor $\alpha = N_3/N_1$, where α is predicted to be 5/7 or 6/7 depending on constitutive assumptions.[2] The values for a_T and b_T reported in Table 1 were determined from the mechanical data alone. In general, there is good agreement between the optical and mechanical dynaic modulus. The poor overlap at high frequencies for the 1,2-PB data (Figure 1B) reflects a failure of the stress-optic rule in the rubber-to-glass transition region due to additional glassy stress relaxation modes at very high frequencies (short time scales).[17] The breakdown of the stress-optic rule in this transition regime does not affect the conclusions of this report since in the blends attention is focused on the rubbery plateau and terminal regions.

The temperature dependences of the pure component a_T values are characterized by the WLF equation:[15]

$$\log a_T = -\frac{C_1^g(T-T_g)}{C_2^g + (T-T_g)} \quad (10)$$

where C_1^g and C_2^g are material constants related to the fractional free volume at T_g and the thermal expansion coefficient of the fractional free volume. For PI ($T_g = -63$ °C by DSC) we find $C_1^g = 13.3$ and $C_2^g = 58$ K, while for 1,2-PB ($T_g = 0$ °C) we find $C_1^g = 12.3$ and $C_2^g = 51.4$ K, which are in reasonable agreement with values reported previously.[4] The WLF coefficients, characterizing the temperature dependence of the relaxation dynamics for the pure components referenced to their respective T_g,

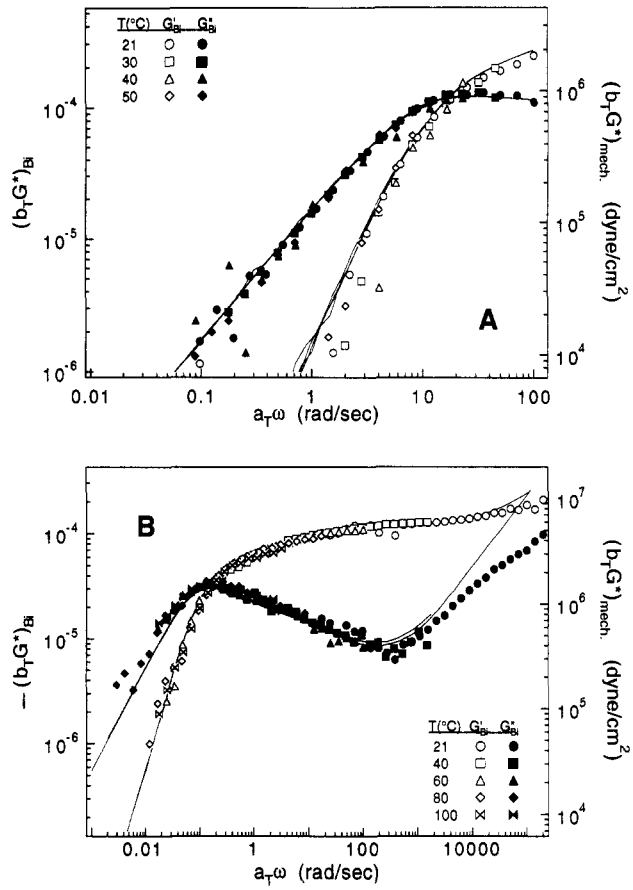

Figure 1. Master curves of the mechanically and optically measured $G^*(\omega)$ for pure components. Mechanical data are represented by the solid lines and optical data are denoted by symbols: (A) G_{Bi}^* and G^* for pure PI, referenced to $T_0 = 21$ °C; (B) $-G_{Bi}^*$ and G^* for pure 1,2-PB, referenced to $T_0 = 60$ °C. Note that negative birefringence results are plotted for 1,2-PB.

Table 1. Stress-Optic Coefficients and Shift Factors for Pure Components

polymer	T (°C)	a_T	b_T	$a_{T,Bi}$	c (cm²/dyn)[a]
PI	21	1	1	1	$1.3_8 \times 10^{-10}$
PI	30	0.47	1.09	0.46	$1.2_8 \times 10^{-10}$
PI	40	0.225	1.18	0.23	$1.2_1 \times 10^{-10}$
PI	50	0.12	1.24	0.11	$1.1_4 \times 10^{-10}$
1,2-PB	21	1200	1.02	1100	$-3.1_5 \times 10^{-11}$
1,2-PB	40	18	1.01	17	$-2.8_6 \times 10^{-11}$
1,2-PB	60	1	1	1	$-2.5_4 \times 10^{-11}$
1,2-PB	80	0.16	0.97	0.17	$-2.2_8 \times 10^{-11}$
1,2-PB	100	0.033	0.97	0.032	$-2.1_3 \times 10^{-11}$

[a] c is the product of the stress-optic coefficient and $\alpha = N_3/N_1$.

are within experimental error the same for the two pure components.

In contrast, each of the pure components exhibits a slightly different b_T temperature dependence (Table 1). In the case of PI, b_T increases appreciably with T, while for 1,2-PB b_T is much less sensitive to temperature and actually decreases slightly with increasing T. This fortuitous disparity enables us to explore the effect of blending on the component $b_T(T)$ behaviors.

Entanglement molecular weights for the pure components are readily available in the literature. For 1,2-PB, Roovers and Toporowski[18] reported $M_{e,PB} = 3800$–3900 on polybutadienes with high vinyl content. For PI, Ferry[15] lists $M_{e,PI} = 6100$ and the results of Gotro et al.[19] give $M_{e,PI} = 6300$. These values are determined from the plateau modulus, G_N°, in accord with rubber elasticity theory:

$$M_e = \frac{\rho RT}{G_N^\circ} \quad (11)$$

where ρ is density and R is the universal gas constant. This relation is used to recover the respective component M_e values in the current blends, and so it is necessary to estimate $G_N°$ for each component. $G_N°$ may be reliably recovered from an integration of the terminal loss modulus, but only if the terminal and rubber-to-glass transition responses are sufficiently separated and the experimental frequency window spans the full relaxation spectrum.[15] Generally, this is only possible with polymers of extremely high molecular weights (i.e., $M > 100M_e$). For moderate molecular weights, however, it has been found[20] that the maximum in the loss modulus, G_m'', remains nearly the same as for higher molecular weights and can thus be used as a measure of $G_N°$. In a study of five nearly monodisperse polymers Raju et al.[20] observed that the ratio of the plateau modulus to the loss maximum appears to be a universal constant:

$$G_N°/G_m'' = q \tag{12}$$

where $q = 3.56$, although the exact value of q will vary slightly as the molecular weight distribution varies. The proportionality of G_m'' and $G_N°$ is assumed to hold in the current blends and so it is necessary to identify q for each of the components. Based on the mechanically obtained loss modulus at 21 °C for the current pure components and the literature M_e values, the q coefficients are determined using eqs 11 and 12: $q_{PI} = 3.89$ and $q_{PB} = 3.87$, which are in reasonable agreement with the findings of Raju. The slightly greater values here are possibly due to a slightly broader molecular weight distribution ($M_w/M_n < 1.05$ for all polymers in the Raju et al. study[20]). Lower molecular weight might also give rise to a higher value of q due to a broadening of the relaxation spectrum associated with contour length fluctuations.

5.0. Blend Dynamics

Typical examples of the component G^* contributions recovered from G^* and G_{Bi}^* using (7) and (9) with $\epsilon = 0.35$ are shown in Figures 2 and 3. For the molecular weights used here, at a given $T - T_g$ pure PI relaxes faster than pure 1,2-PB. Consequently, the high-frequency (short time scale) features of the blend dynamic modulus are expected to be primarily due to PI relaxation, while the low-frequency (long time scale) features are expected to be associated with 1,2-PB relaxation. This hypothesis is verified by inspection of the recovered component contributions and was proved conclusively by the dichroism measurements reported in ref 2.

The general shape of the G_{PI}^* response is much like that of a pure monodisperse homopolymer: there is a single plateau in G_{PI}' and a single maximum in G_{PI}''. On the other hand, G_{PB}' and G_{PB}'' take on slightly more complex shapes than those of a pure melt. The deviations in G_{PB}' and G_{PB}'' are highly correlated with the PI relaxation and are attributed to constraint release mechanisms. On a time scale less than the PI characteristic relaxation time (corresponding to high ω), the stress experienced by the 1,2-PB chains arises due to confinement imposed by entanglements with other 1,2-PB chains as well as with PI chains. At times greater than the PI relaxation time, the PI chains have essentially completely undergone stress relaxation, reflecting that they have had sufficient time to diffuse out of the original chain entanglements in which they participated on shorter time scales. A consequence of this is that the PI chains have released their constraints on the 1,2-PB chains at these longer times. According to rubber elasticity theory, the modulus amplitude is directly proportional to the density of entanglements. Thus, in passing from high ω to lower ω, the 1,2-PB chains experience a reduction of effective entanglements (due to PI relaxation), leading to the observed decrease in the 1,2-PB dynamic modulus. This constraint release effect is discussed more quantitatively below.

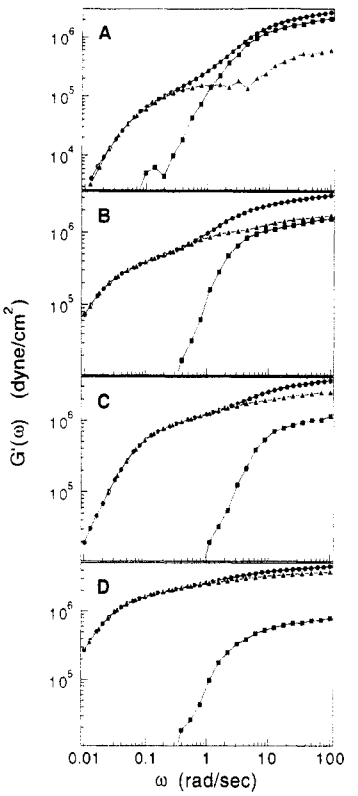

Figure 2. Blend and component storage moduli: (A) 20% 1,2-PB at 21 °C; (B) 40% 1,2-PB at 21 °C; (C) 60% 1,2-PB at 40 °C; (D) 80% 1,2-PB at 40 °C. Symbols correspond to (●) mechanically acquired G', (■) G_{PI}' using $\epsilon = 0.35$, and (▲) G_{PB}' using $\epsilon = 0.35$.

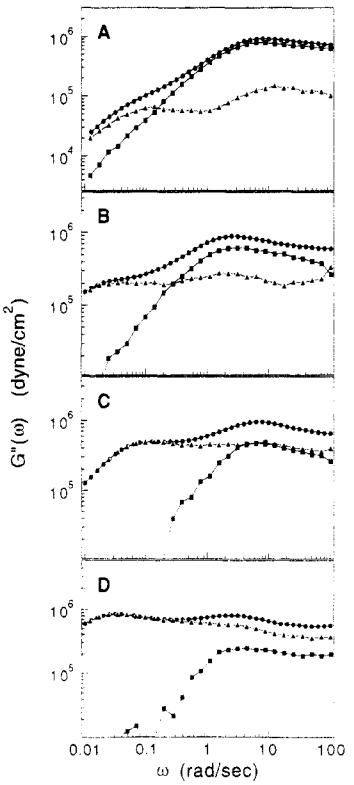

Figure 3. Blend and component loss moduli: (A) 20% 1,2-PB at 21 °C; (B) 40% 1,2-PB at 21 °C; (C) 60% 1,2-PB at 40 °C; (D) 80% 1,2-PB at 40 °C. Symbols correspond to (●) mechanically acquired G'', (■) G_{PI}'' using $\epsilon = 0.35$, and (▲) G_{PB}'' using $\epsilon = 0.35$.

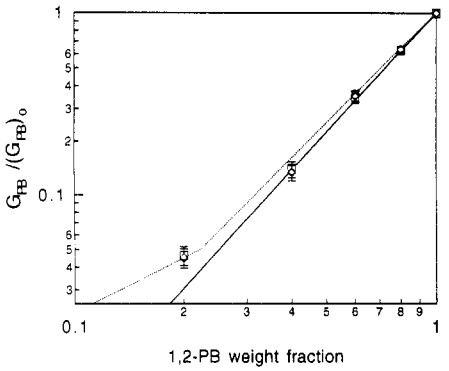

Figure 4. Composition dependence of the normalized loss maximum (□) and crossover amplitude (◇) of G_{PB}* in the low-frequency region at 21 °C. The solid line has a slope of 2.18, and the dotted line corresponds to constraint release scaling predictions.

To assess the effects of blending on the rheology of each component, an analysis of the component G^* contributions is conducted analogously to that employed with homopolymers. This analysis focuses on both the frequency and magnitude characteristics of the component moduli, concentrating on how they vary with temperature and blend composition. Interpretation of the frequency behavior of the dynamic modulus yields a characteristic relaxation time for each component, while the modulus level is related to the density of chain entanglements. From these properties additional insight may then be recovered regarding the monomeric friction factors of the blend components.

5.1. Component Modulus Magnitudes and Chain Entanglements. Analysis of the magnitudes of the component G^* responses provides a means of investigating current notions regarding (1) constraint release and dilution in multicomponent polymer systems, (2) the composition dependence of the entanglement density and reptation tube diameter for each component in a miscible blend, and (3) the nature of the modulus shift factor b_T. These topics are discussed sequentially in the following sections.

5.1.1. Composition Dependence of 1,2-PB Modulus in the Terminal Region. We focus first on the low-frequency regime, where the dynamic modulus is dominated by the 1,2-PB contribution, which in turn is expected to be governed by entanglements of 1,2-PB chains with other 1,2-PB chains only. The maximum in the loss modulus $G''_{m,PB}$ and the crossover amplitude $G^*_{G'=G'',PB}$ in this longer time scale region are used to characterize the amplitude of the modulus, rather than using the plateau in G'_{PB} (made difficult, as usual, by the slope of the storage modulus in the rubbery zone) or attempting to integrate under the loss modulus (made difficult by the proximity of the higher frequency regime, where G_{PB} consists of additional contributions associated with the constraints imposed by 1,2-PB entanglements with unrelaxed PI chains). In the low-ω regime it is assumed that, as in the pure component state, the maximum in the 1,2-PB loss modulus serves as a measure of the plateau modulus of the 1,2-PB chains after the PI chains have relaxed, scaled by a constant (see eq 12).[20] Shown in Figure 4 are the loss maxima and crossover magnitudes of G_{PB}* in the low-frequency region at 21 °C. To facilitate comparison, the data are normalized by the pure 1,2-PB values. Comparison is made at constant temperature rather than at constant $T - T_g$, since the plateau modulus is governed by the density of chain entanglements, which varies with absolute T, not $T - T_g$ (see eq 11). The error bars in Figure 4 and throughout this report correspond to the uncertainty associated with the stress-optic coefficients used in the analysis. The effects of other factors found to be less influential,[2] such as the assumed value for the coupling coefficient and the assumption of composition-invariant stress-optic coefficients, are not included.

Over most of the composition range, the data closely followed a ϕ_{PB}^{α} scaling with an exponent of $\alpha = 2.2$. This behavior closely resembles that of highly entangled polymers diluted with solvents. In such systems experiments indicate

$$G_N^\circ \sim \phi_{polymer}^{\alpha} \tag{13}$$

at all compositions within the concentrated polymer solution regime, where reported values of α vary slightly with polymer species but remain within the range of 2.0–2.3.[21] The data in Figure 4 obey the power law of eq 13 with $\alpha = 2.2$, except at 20% 1,2-PB, where the modulus magnitude is significantly larger. A similar observation was made by Struglinski and Graessley[22] in binary mixtures of nearly monodisperse 1,4-polybutadiene components with distinct molecular weights ($M \gg M_e$ for both components) and is suggestive of a constraint release mechanism. To compare the current results to constraint release predictions, we consider the scaling predictions of the theory by Doi, Graessley, Helfand, and Pearson[23] and that by Viovy, Rubinstein, and Colby,[24] which turn out to be identical for the molecular weights and entanglement molecular weights of the components used here.

To evaluate the composition dependence of the slower relaxing component's G^* magnitude, it is necessary to first assess whether constraint release reduces the relaxation time of the slower component. According to the mentioned theories, the relaxation time of the slower component is not affected by constraint release if relaxation of the chain by reptation is faster than the Rouse relaxation of the confining tube, which translates to the following criterion for a miscible polymer blend:

$$\frac{\tau_{Rouse}^{tube}}{\tau_{reptation}^{chain}} \approx \frac{\left(\zeta_{0,S} b_S^2 \frac{N_S^3}{N_{e,S}}\right)\left(\frac{N_L^2}{N_{e,L}^2}\right)}{\zeta_{0,L} b_L^2 \frac{N_L^3}{N_{e,L}}} = \left(\frac{\zeta_{0,S} b_S^2}{\zeta_{0,L} b_L^2}\right)\frac{N_S^3}{N_L N_{e,S} N_{e,L}} > 1 \tag{14}$$

where the subscript S corresponds to the component with the shorter relaxation time and L to the one with the longer relaxation time. ζ_0 is the monomeric friction factor, N is the number of segments per chain, b is the segment length, and N_e is the average number of segments between chain entanglements (note that for the case of bidisperse homopolymers this condition reduces to the more familiar form: if $M_S^3/(M_L M_e^2) > 1$, then chain reptation dominates Rouse relaxation of the tube). Diffusion studies on polystyrene suggest that the ratio in (14) must exceed approximately 10 rather than unity to safely neglect the effects of constraint release on the relaxation time of the slower relaxing component.[25] For the PI/1,2-PB blend studied here, this ratio is approximately 120, and so 1,2-PB is expected to relax by normal chain reptation. Consequently, its relaxation time is not reduced in the blend since contraints with the faster relaxing component do not vanish quickly enough. As will be discussed below, no reduction in τ_{PB} is observed with increasing PI content (to the contrary, a slight increase is observed).

Within this so-called dilation-free regime, the slower relaxing component's modulus follows one of two different

Table 2. Characteristic Modulus Amplitudes and Entanglement Spacings

1,2-PB frac (wt %)	$G_m''_{PI}$ (dyn/cm²)	$N_{e,PI}$	low ω $G_m''_{PB}$ (dyn/cm²)	low ω $N_{e,PB}$	$(G'_{PB})^{high\ \omega}/(G'_{PB})^{low\ \omega}$	high ω $N_{e,PB}$
0	9.1×10^5	360				
20	7.7×10^5	340	0.68×10^5	610	2.8	220
40	6.3×10^5	310	2.1×10^5	400	1.9	210
60	4.7×10^5	280	5.0×10^5	250	1.4	180
80	2.4×10^5	270	(9.0×10^5)	(180)	1.1	(160)
100			(14.5×10^5)	(142)		

behaviors, depending on blend composition. These two zones correspond to the ND wedge and ND box in Doi[23] terminology and chain reptation I and II in Viovy[24] terminology. The blend composition at which the two cases meet is given by

$$\phi_L^* = \left(\frac{\tau^S_{reptation}}{\tau^L_{reptation}}\right)^{1/2} = \left[\frac{\zeta_{0,S} b_S^2}{\zeta_{0,L} b_L^2}\left(\frac{N_S}{N_L}\right)^3\left(\frac{N_{e,L}}{N_{e,S}}\right)\right]^{1/2} \quad (15)$$

For the current system $\phi_{PB}^* \approx 0.22$. For blend compositions greater than ϕ_{PB}^*, G_{PB}^* is predicted to scale according to the simple dilution rule ($G_{PB}^* \sim \phi_{PB}^2$), while below ϕ_{PB}^*, G_{PB}^* is expected to scale as $\phi_{PB}\phi_{PB}^*$. These predictions, shown in Figure 4, are consistent with the data, though a comprehensive assessment of the model predictions cannot be made due to the lack of sufficient data at low 1,2-PB compositions.

5.1.2. Composition Dependence of Entanglements and Tube Diameters. In the higher frequency region of the dynamic modulus, where the temporary network is comprised of the chain entanglements experienced by both PI and 1,2-PB, it is of interest to evaluate the modulus amplitude for each component. The PI modulus amplitude is easily characterized by $G_{m,PI}''$ and $G_{G'=G'',PI}^*$. However, for 1,2-PB a more involved approach is necessary. A rough estimate of the G_{PB}^* amplitude at high ω is made by studying the increase in G_{PB}' for the low-to high-ω regions. The estimated shift in G_{PB}' is multiplied by $G_{m,PB}''$ recovered at low ω and the product is used as a rough measure of the 1,2-PB modulus amplitude at high ω. At high ω, G_{PB}' has a rather well defined and small slope; however, in the lower ω region G_{PB}' tends to be somewhat steeper and more rounded (see Figure 2), making these estimates for 1,2-PB reliable only to within about ±15%. Values characterizing the modulus amplitude of each component are given in Table 2.

It is instructive to use these values to assess the entanglement spacing of each component as a function of blend composition. Assuming again that G_m'' is related to G_N° by (12), the number of backbone bonds in an entanglement strand may be calculated for component i by

$$N_{e,i} = \frac{M_{e,i}}{m_{0,i}} = \frac{\phi_i \rho_i RT}{q m_{0,i} G_{m,i}''} \quad (16)$$

where $m_{0,i}$ is the molecular weight per backbone bond for component i. These values are given in Table 2 and are plotted in Figure 5. Pure 1,2-PB experiences approximately twice as many entanglements per unit volume compared to pure PI. As a result, it is anticipated that with increasing ϕ_{PB} both components should experience a reduction in N_e (in the high-ω region). Such behavior is exhibited by both components.

Tsenoglou proposed a model for the composition dependence of the entanglements experienced by each blend component based on pure component entanglement

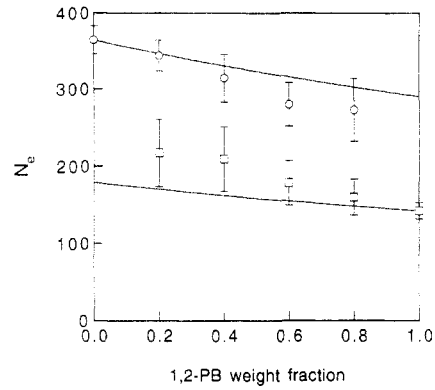

Figure 5. Composition dependence of the average number of chemical bonds between entanglements for each component in the high-frequency region at 21 °C: (○) $N_{e,PI}$; (□) $N_{e,PB}$. Lines correspond to the predictions of the Tsenoglou theory.

weights:[26]

$$M_{e,i} = \frac{M_{e,i_0}}{\phi_i + \phi_j\left(\frac{\rho_j M_{e,i_0}}{\rho_i M_{e,j_0}}\right)^{1/2}} \quad (17)$$

This blend M_e model assumes only that randomness prevails in the distribution of inter- and intracomponent entanglements and the presence of the unlike component does not alter the ability of a chain to participate in entanglements. The lines in Figure 5 correspond to the Tsenoglou theory predictions, using (17) and $N_e = M_e/m_0$. Previously, only the Tsenoglou prediction for the overall blend plateau modulus could be tested. Here, the theory may be more rigorously assessed by checking its predictions for each component. Agreement between the data and the model is quite good. These observations demonstrate that separate entanglement molecular weights for each species in a miscible polymer blend are indeed possible. As suggested by the Tsenoglou model, this is primarily due to differences in the flexibility of each component.

The component entanglements may be alternatively studied in terms of reptation tube diameters. In the reptation theory the diameter of the hypothetical tube confining a given chain, a, is related to the spacing between entanglements and may be written as

$$a = (C_\infty N_e)^{1/2} b_0 \quad (18)$$

where C_∞ is the Flory characteristic ratio[27] (C_∞ = 5.2 for PI and 7.0 for 1,2-PB)[18,28] and b_0 is the average skeletal bond length (1.47 Å for PI and 1.54 Å for 1,2-PB).[21] Component tube diameters calculated with this expression are shown in Figure 6 along with predictions based on the Tsenoglou theory. Unfortunately, because C_∞ and b_0 for 1,2-PB are slightly larger than for PI, the disparity between the pure component tube diameters is much less than the difference in their N_e values, making it difficult to determine whether each component in the blend experiences a distinct tube diameter. Within experimental error, though, the simplest notion of a common tube appears to be at least a fair approximation for this blend.

5.1.3. Temperature Dependence of Modulus. In addition to studying the composition dependences of the component G^* amplitudes, it is worth investigating their temperature dependences. As mentioned earlier, the pure components have G^* amplitudes which vary differently with temperature. This is manifest by their distinct $b_T(T)$ behaviors observed by mechanical rheometry (Table 1). The strong temperature dependence of b_T for PI was verified with different rheometer plate geometries and

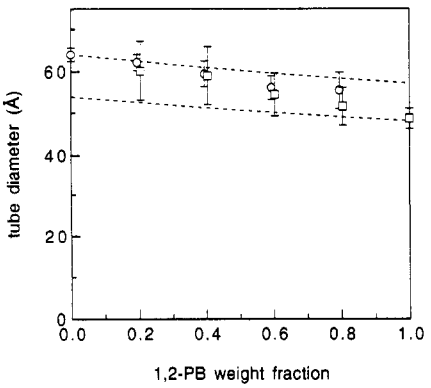

Figure 6. Composition dependence of reptation tube diameters for each component based on component N_e values: (○) a_{PI}; (□) a_{PB}. The data are slightly offset for clarity. The dashed lines correspond to the predictions of the Tsenoglou theory.

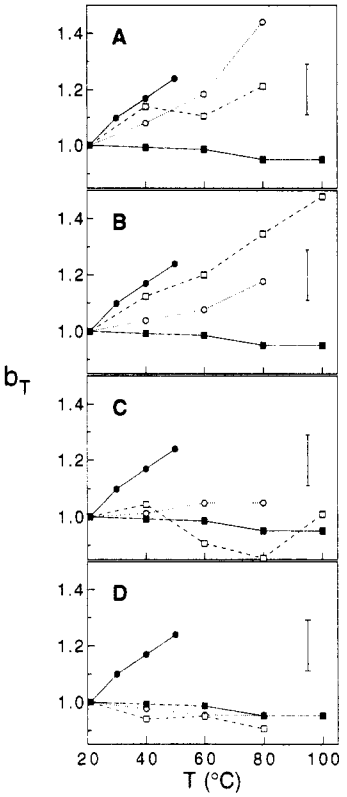

Figure 7. Modulus shift factors, b_T, for each component in the blend and pure state referenced to 21 °C: (●) pure PI; (■) pure 1,2-PB; (○) PI in the blend; (□) 1,2-PB in the blend. (A) 20% 1,2-PB; (B) 40% 1,2-PB; (C) 60% 1,2-PB; (D) 80% 1,2-PB. For comparison all plots show the pure component behavior. A typical error bar is shown to the right in each plot.

for temperatures extending down to −38 °C. In the blend, modulus shift factors for each component are calculated using the ratio of either the crossover magnitude ($G_{G'=G''}$*) or the loss modulus maximum (G_m''), at a given temperature, to the value at 21 °C (note that b_T computed for 1,2-PB corresponds to its low-frequency behavior). Good agreement is observed between the values calculated by the two approaches; here we report the average. The modulus shift factors for each component at the four blend compositions studied are shown in Figure 7 along with the pure component b_T factors for comparison. Although the temperature range is rather limited, an interesting trend is evident. In the pure state each component exhibits a distinct b_T temperature dependence. However, in the blend a mutual behavior appears to arise. Moreover, the unified blend b_T behavior more closely resembles that of the more abundant blend component. Such behavior indicates that the blend environment has a strong influence on the temperature dependence of whatever parameters govern the plateau modulus.

We anticipate the temperature dependence of the modulus to be given by eq 11 for the plateau modulus

$$b_T = \frac{(G_N^\circ)_T}{(G_N^\circ)_{T_0}} = \frac{(\rho T/M_e)_T}{(\rho T/M_e)_{T_0}} = \frac{(\rho T/a^2)_T}{(\rho T/a^2)_{T_0}} \tag{19}$$

The last result was obtained from $M_e = m_0(a/b_0)^2$, with m_0 and b_0 being temperature independent. If the tube diameter a is independent of temperature, this reduces to the well-known Rouse result[1] of $b_T = (\rho T)_T/(\rho T)_{T_0}$. However, the Rouse result does not even work for the two pure components, since they have very similar thermal expansion coefficients and disparate temperature dependences for b_T. Thus, we can conclude that the tube diameter is temperature dependent.

This fact has been well-reorganized in the literature, and a number of ideas have been suggested for the temperature dependence of the modulus. These ideas all have b_T being some function of density ρ, temperature T, and chain statistics, usually cast in terms of the Flory characteristic ratio[27] C_∞. Examples are the Graessley–Edwards[21] form ($b_T \sim \rho^\alpha T C_\infty^{2\alpha-3}$, where α is the exponent for the concentration dependence of G_N°; see eq 13) and the forms suggested by Ronca[29] ($b_T \sim \rho^3 T C_\infty^3$) and Wu[30] ($b_T \sim \rho T C_\infty^{-2}$). These approaches can explain the different b_T temperature dependences of the two pure components, even though their thermal expansion coefficients are essentially the same, by invoking different temperature dependences of C_∞. The temperature dependence of chain statistics is determined by the temperature-dependent energetics of bond rotation,[27] which could easily be different for the two components.

However, these approaches cannot explain the apparent correlation of the temperature dependence of b_T for the two components in the blends (see Figure 7). We do not yet fully understand the observed $b_T(T)$ behaviors of the individual components, but it seems unlikely that the two species adopt a mutual temperature dependence of C_∞, as the current view of chain statistics[27] makes C_∞ a single-chain property, dependent on bond rotation energetics, but independent of the chain's surroundings. While chain statistics in miscible blends has not been studied in detail, there is no reason to suspect that the presence of a different neighboring chain should have an effect on C_∞. On the other hand, it is quite plausible that the tube diameter a is a function of the surroundings, since topological constraint necessarily involves both the individual chain and its neighbors. The mutual behavior of $b_T(T)$ for the two components in the blend, demonstrated in Figure 7, suggests that the tube diameters of the two components have the same temperature dependence (see eq 19). Coupled with the apparent identical composition dependence of the two tube diameters (Figure 6), we make the tentative conclusion that the two components of a miscible blend share a single common tube.

5.2. Component Relaxation Times and Friction Factors. 5.2.1. Component Relaxation Times. Even before an effort is made to explicitly identify the blend component relaxation times, insight into the temperature dependences of the component relaxation dynamics may be acquired by investigating how the moduli shift along the frequency axis with varying temperature. Roovers and Toporowski[4] observed that the overall dynamic modulus in blends of PI and 1,2-PB does not lend itself to time–temperature superposition due to the clearly distinct temperature dependences of the relaxation features of G^* associated with each component. Such

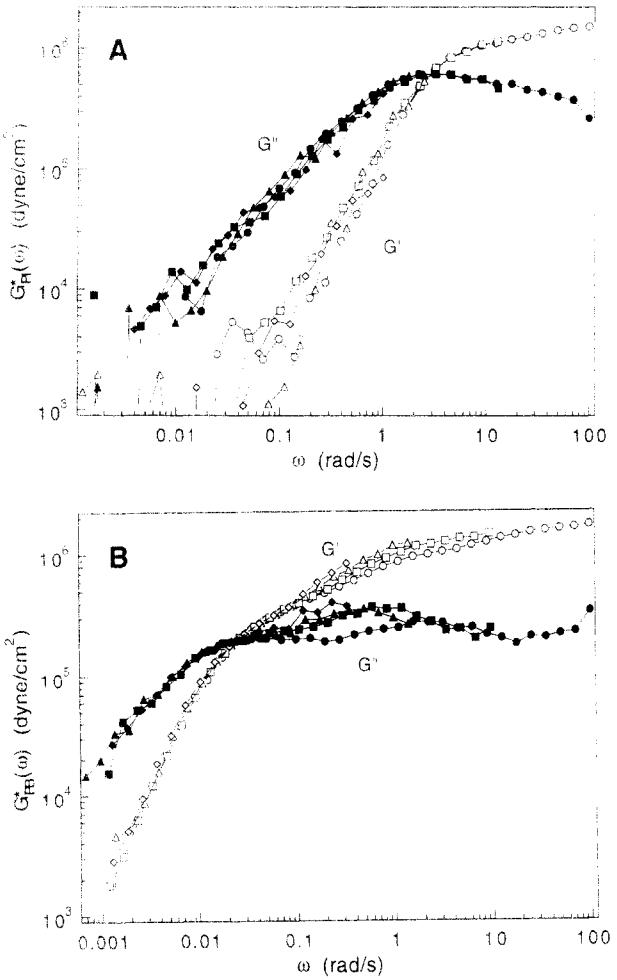

Figure 8. Time–temperature superposition of component moduli for the 40% 1,2-PB blend, referenced to 21 °C: (A) G_{PI}*; (B) G_{PB}*.

thermorheological complexity in miscible polymer blends was also noted in blends of poly(ethylene oxide) and poly(methyl methacrylate)[31,32] and blends of 1,2-polybutadiene and 1,4-polybutadiene.[33] Our mechanically obtained G^* confirm the failure of the time–temperature superposition principle for the PI/1,2-PB blends. Although the overall blend does not follow a single temperature dependence, it might still seem reasonable to expect each of the blend components to separately obey the time–temperature superposition principle with unique shift factors, permitting the generation of separate component master curves. Roovers and Toporowski could not test this from measurements of the blend G^* alone. Our results indicate that time–temperature superposition does indeed hold for PI, as shown in Figure 8A. On the other hand, superposition of the 1,2-PB curves over the entire dynamic range cannot be realized since the high-frequency 1,2-PB relaxation features are correlated with PI relaxation, which follows a separate temperature behavior. Thus, only in the terminal region is reasonable superposition observed for 1,2-PB (see Figure 8B).

To study the unique temperature dependences of the component relaxation dynamics more quantitatively, the characteristic relaxation time τ for each species is recovered. From the blend G^* Roovers and Toporowski[4] estimated τ_{PI} and τ_{PB}. Here, these values may be more confidently recovered from the individual component G^*, taking the reciprocal of the crossover frequency (i.e., ω at which $G' = G''$) in the terminal zone of each component to be its characteristic relaxation time. Component relaxation times are given in Table 3. Uncertainty in these values (mainly due to uncertainty in the stress-optic

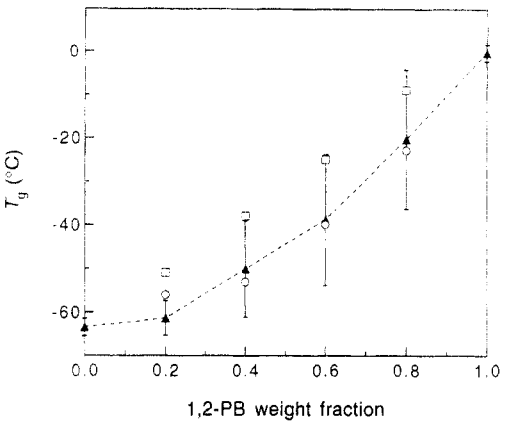

Figure 9. Blend glass transition temperatures: (▲) DSC results; (○) effective PI T_g recovered from WLF analysis; (□) effective 1,2-PB T_g. Bars indicate the breadth of the transition observed by DSC.

Table 3. Blend Component Relaxation Times

1,2-PB frac (wt %)	T (°C)	τ_{PI} (s)	τ_{PB} (s)	1,2-PB frac (wt %)	T (°C)	τ_{PI} (s)	τ_{PB} (s)
0	21	0.062		60	21	1.7	170
0	30	0.029		60	40	0.13	10.8
0	40	0.014		60	60	0.032	1.6
0	50	(0.0075)		60	80	(0.006)	0.38
20	21	0.25	9.5	60	100	(0.002)	0.10
20	40	0.40	1.3	80	21	4.4	(800)
20	60	0.010	0.29	80	40	0.49	36
20	80	(0.003)	0.08	80	60	0.08	3.3
40	21	0.38	43	80	80	0.025	0.10
40	40	0.045	4.1	100	21		(9000)
40	60	(0.008)	0.62	100	40		135
40	80	(0.002)	0.14	100	60		7.5
40	100	(<0.001)	0.048	100	80		1.2
				100	100		0.25

coefficients) is roughly 15% or less. The temperature dependences of these relaxation times are characterized by a WLF analysis. As Roovers and Toporowski pointed out, given the similarity in the pure component WLF coefficients, it seems plausible to expect these parameters to remain the same upon blending, when referenced to the blend T_g. To identify the blend T_g, we follow their approach, in which C_2^g for each component in the blend is assumed to be the mean value of the pure components, 55 K (C_1^g need not be specified to determine T_g). WLF behavior dictates that plots of $\log\tau$ *vs* $1/(T-(T_g-C_2^g))$ are linear, and thus, the effective T_g of each component is taken to be the T_g value which yields the minimum least squares deviation from linearity for such a plot. The component relaxation times are found to yield good linearity in these plots; however, due to the rather mild curvature which arises when values close to T_g are used, it is possible to assess the component T_g's only to about ±5 °C. Reliability of the recovered T_g values is confirmed by the two alternate methods described by Roovers and Toporowski,[4] one based on specification of both C_1^g and C_2^g, and the other based on the superposition of $\log a_T$ *vs* T curves.

From this analysis effective component glass transition temperatures differing by as much as 16 °C are found at a given composition. These values along with the DSC results are plotted in Figure 9. Note that the 1,2-PB T_g is greater than that of PI for all compositions, indicating that 1,2-PB chains require a higher temperature (or equivalently, greater fractional free volume) to undergo the transition from glass to melt. As a result, although the relaxation processes of both components may be scaled according to the same WLF parameters, the fact that they exhibit distinct T_g's gives rise to differing absolute

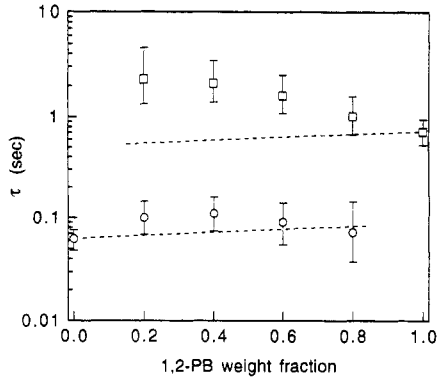

Figure 10. Component relaxation times as a function of composition at $T - T_g = 85$ °C: (○) τ_{PI}; (□) τ_{PB}. Dashed lines correspond to the expected variation in τ due to changes in M_e.

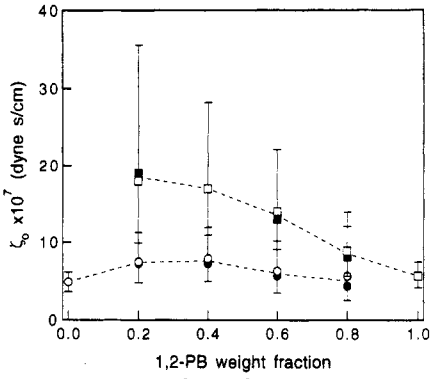

Figure 11. Composition dependence of component friction factors at $T - T_g = 85$ °C based on reptation theory using experimentally recovered relaxation times and entanglement molecular weights: (○) $\zeta_{0,PI}$; (□) $\zeta_{0,PB}$. For comparison values are also calculated using Tsenoglou theory predictions of M_e: (●) $\zeta_{0,PI}$; (■) $\zeta_{0,PB}$.

temperature dependences. In general, the component T_g's differ by an amount comparable to the breadth of the overall transition observed by DSC, and except at very low 1,2-PB volume fractions the component values lie within the DSC transition range. This discrepancy may be due in part to the fact that these calculated T_g's lie farthest from the temperature range at which the rheological experiments were conducted. These observations are in agreement with the findings of Roovers and Toporowski,[4] supporting their conclusion that the origin of the thermorheological complexity lies in the unique glass transition temperatures experienced by each of the blend components.

The effect of blend composition on the component relaxation processes is investigated by focusing on the component relaxation times at a fixed $T - T_g$ so that the comparisons are made on approximately an iso-free volume basis. Figure 10 shows the composition dependences of the component relaxation times at $T - T_g = 85$ °C, using the effective component T_g values. With increasing 1,2-PB content, τ_{PB} decreases steadily while τ_{PI} varies only mildly. Roovers and Toporowski observed the same trends. Due to the high number of entanglements encountered by each species, constraint release effects are not expected to affect τ_{PB} in the current system; however, the difference in the entanglement densities of the pure components is expected to have an influence on the relaxation times of both species. As mentioned above, since pure 1,2-PB is more highly entangled than PI, relaxation for both species is expected to be more hindered in the 1,2-PB-rich blends. Such behavior is qualitatively observed for PI, but not for 1,2-PB. An estimate of the extent to which the entanglement effect should influence component relaxation times may be made by using the tube model prediction $\tau \sim 1/M_e$ and the Tsenoglou theory prediction for the composition dependence of M_e (see eq 17). The dashed lines in Figure 10 correspond to these predictions, and it can be seen that τ_{PI} qualitatively follows this behavior. It is not possible to say whether the apparent maximum in τ_{PI} at $\phi_{PB} = 0.4$ is real or merely an artifact due to the uncertainty in τ_{PI} and the effective T_g values for PI. On the other hand, the 1,2-PB composition dependence takes on a completely different behavior over the full composition range, as τ_{PB} tends to increase with PI dilution rather than decrease. There are several possible effects which may be responsible for this discrepancy, including the uncertainty in assessing $T_{g,PB}$, the the applicability of using constant $T - T_{g,PB}$ as an iso-free-volume state and the possibility of composition-dependent friction factors, which is discussed in the following section.

5.2.2. Component Friction Factors. The composition dependence of the blend component dynamics may be alternatively analyzed in terms of monomeric friction factors. Estimates of component friction factors are presented here based on the tube model, using the experimentally recovered relaxation times and entanglement molecular weights. Since tube dilation does not affect the relaxation dynamics for the molecular weights used here, the values for $M_{e,PB}$ at high ω are used. For comparison the calculations are also performed using the Tsenoglou theory predictions for M_e. According to the tube model, the monomeric friction factor ζ_0 is related to the characteristic relaxation time by[1]

$$\tau = \frac{\zeta_0 N^3 b^2}{\pi^2 k_b T}\left(\frac{b}{a}\right)^2 = \frac{\zeta_0 N^2 b^2}{\pi^2 k_b T}\frac{M}{M_e} \tag{20}$$

where a is the tube diameter, b is the Kuhn segment length, N is the number of segments per chain, and k_b is Boltzmann's constant. Component friction factors recovered in this fashion at constant $T - T_g$ (using the effective component T_g's) are plotted in Figure 11. Due to the uncertainty in the component T_g values, which affects values for τ, caution must be exercised in drawing conclusions from the friction factor calculations. With this in mind, it is only possible to safely make the qualitative observation that $\zeta_{0,PB}$ increases appreciably in the presence of PI but that $\zeta_{0,PI}$ is, at best, only mildly affected by the presence of 1,2-PB. At 20% 1,2-PB $\zeta_{0,PB}$ is 3 times larger than the pure 1,2-PB value.

These trends in the calculated friction factors have significant implications regarding the applicability of the simple ζ_0 blend rule suggested by Brochard-Wyart.[34] This model proposes that the two component friction factors in a binary miscible blend are governed by three coefficients, $\zeta_{PI,PI}$, $\zeta_{PB,PB}$, and $\zeta_{PI,PB}$, which characterize segmental friction between PI and PI chains, 1,2-PB and 1,2-PB chains, and PI and 1,2-PB chains, respectively:

$$\begin{aligned}\zeta_{0,PI} &= \phi_{PI}\zeta_{PI,PI} + \phi_{PB}\zeta_{PI,PB}\\ \zeta_{0,PB} &= \phi_{PI}\zeta_{PI,PB} + \phi_{PB}\zeta_{PB,PB}\end{aligned} \tag{21}$$

In accord with the model, the calculated component friction factors for the current system are (within experimental uncertainty) approximately linearly dependent on composition. However, the model also predicts that both components should have the same infinite dilution ζ_0 since interchain friction is assumed to be described by a single coefficient. In other words, as $\phi_{PB} \to 0$, the value of $\zeta_{0,PB}$ should approach $\zeta_{PI,PB}$; and likewise, as $\phi_{PB} \to 1$ $\zeta_{0,PI}$ should approach the same $\zeta_{PI,PB}$. From Figure 11 this is clearly not the case for the current results. The apparent trends suggest that interchain friction is not symmetric and might

then be more appropriately described by two separate coefficients ($\zeta_{PI,PB}$ and $\zeta_{PB,PI}$) rather than one. Indeed, a better fit to the data cuold be achieved with a four-parameter model rather than three.

The composition dependences of the calculated friction factors here are not nearly as dramatic as those reported in blends of polystyrene/poly(xylenyl ether), based on forward recoil spectrometry measurements of tracer diffusion coefficients.[35] In that blend of polymers with bulkier repeat units, friction factors at constant $T - T_g$ were observed to increase by more than an order of magnitude in the blend. Thus, the comparatively mild composition dependences of the calculated friction factors for the current system of less bulky, noninteracting species do not seem unreasonable and are likely to be responsible for the apparent increase of τ_{PB} upon blending (see Figure 10), seen also by Roovers and Toporowski.[4] However, further investigation of the component friction factors is warranted to substantiate this hypothesis.

6.0. Summary

Separation of $G^*(\omega)$ into component contributions based on complementary dynamic mechanical rheometry and polarimetry has proven to be a valuable tool in assessing the effects of blending on the rheology of each component in the nearly ideal mixtures of PI and 1,2-PB. In general, reliable recovery of component contributions to the modulus amplitude is not possible based on mechanical measurements alone. In this regard, the use of a complementary rheo-optical technique is particularly rewarding. Our results indicate that for the molecular weights studied here the faster relaxing component, PI, influences the modulus of the slower relaxing component, 1,2-PB, in a fashion similar to a solvent diluent over much of the composition range. For the blend richest in PI, however, evidence of an additional mode of relaxation (i.e., constraint release) was observed. The scaling predictions of two constraint release theories originally developed for homopolymer melts of bimodal molecular weight distribution were found to describe the trends reasonably well. Based on the component modulus amplitudes in the high-ω region, we conclude that each species has an individual entanglement molecular weight in the blend, in agreement with the Tsenoglou blend entanglement theory. Unfortunately, because the pure component tube diameters are not widely separated, it is not possible to definitely prove whether a single tube diameter arises upon blending, although our data are consistent with this simple idea. Investigation of the component moduli at different temperatures shows a merging of the component modulus temperature dependences to form a single blend $b_T(T)$ behavior, also consistent with the notion of a mutual tube.

Findings on relaxation times recovered from the component $G^*(\omega)$ contributions confirm that relaxation of each species is governed by a distinct effective glass transition. Comparing relaxation times to pure component values at a given $T - T_g$ verifies that in this blend of negligible specific interactions relaxation times are only mildly influenced by the second component. These trends in component relaxation times are consistent with those recovered by mechanical rheometry measurements by Roovers and Toporowski.[4] In the case of PI the mild increase of τ in the blend is in agreement with the enhancement of entanglements due to the presence of 1,2-PB. On the other hand, for 1,2-PB the observed increase on τ suggests a possible increase in its friction factor when blended with PI.

These observations on the PI/1,2-PB blend provide significant insight into miscible blend rheology and demonstrate several concepts essential to the development of a molecular-based theory. The promising results encourage further experimental work. Investigating other PI/1,2-PB molecular weight ratios would be interesting to test the conclusions drawn from the results on the particular system studied here. Also, studies on other blend systems, including ones with enthalpic interactions, would be useful to assess the generality of our observations.

Acknowledgment. We are thankful for the financial support provided by Eastman Kodak Co., the National Science Foundation (Grant DMR 9120360), and the Center for Materials Research at Stanford University.

References and Notes

(1) Doi, M.; Edwards, S. F. *The Theory of Polymer Dynamics*; Oxford University Press: Oxford, 1986.
(2) Zawada, J. A.; Fuller, G. G.; Colby, R. H.; Fetters, L. J.; Roovers, J. *Macromolecules*, preceding paper in this issue.
(3) Roland, C. M. *Macromolecules* **1987**, *20*, 2557.
(4) Roovers, J.; Toporowski, P. M. *Macromolecules* **1992**, *25*, 3454.
(5) Miller, J. B.; McGrath, K. J.; Roland, C. M.; Trask, C. A.; Garroway, A. N. *Macromolecules* **1990**, *23*, 4543.
(6) Trask, C. A.; Roland, C. M. *Macromolecules* **1989**, *22*, 256.
(7) Roland, C. M. *J. Polym. Sci., Polym. Phys. Ed.* **1988**, *26*, 839.
(8) Tomlin, D. W.; Roland, C. M. *Macromolecules* **1992**, *25*, 2994.
(9) Trask, C. A.; Roland, C. M. *Polym. Commun.* **1988**, *29*, 332.
(10) Kawahara, S.; Akiyama, S.; Ueda, A. *Polym. J.* **1989**, *21*, 221.
(11) Hasegawa, H.; Sakurai, S.; Takenaka, M.; Hashimoto, T.; Han, C. C. *Macromolecules* **1991**, *24*, 1813.
(12) Sakurai, S.; Jinnai, H.; Hasegawa, H.; Hashimoto, T.; Han, C. C. *Macromolecules* **1991**, *24*, 4839.
(13) Kornfield, J. A.; Fuller, G. G.; Pearson, D. S. *Rheol. Acta* **1990**, *29*, 105.
(14) Kornfield, J. A.; Fuller, G. G.; Pearson, D. S. *Macromolecules* **1989**, *22*, 1334.
(15) Ferry, J. D. *Viscoelastic Properties of Polymers*, 3rd ed.; Wiley: New York, 1980.
(16) Doi, M.; Pearson, D.; Kornfield, J.; Fuller, G. G. *Macromolecules* **1989**, *22*, 1488.
(17) Read, B. E. *Polymer* **1964**, *5*, 1.
(18) Roovers, J.; Toporowski, P. M. *Rubber Chem. Technol.* **1990**, *63*, 734.
(19) Gotro, J. T.; Graessley, W. W. *Macromolecules* **1984**, *17*, 2767.
(20) Raju, V. R.; Menezes, E. V.; Marin, G.; Graessley, W. W.; Fetters, L. J. *Macromolecules* **1981**, *14*, 1668.
(21) Graessley, W. W.; Edwards, S. F. *Polymer* **1981**, *22*, 1329.
(22) Struglinski, M. J.; Graessley, W. W. *Macromolecules* **1985**, *18*, 2630.
(23) Doi, M.; Graessley, W. W.; Helfand, E.; Pearson, D. *Macromolecules* **1987**, *20*, 1900.
(24) Viovy, J. L.; Rubinstein, M.; Colby, R. H. *Macromolecules* **1991**, *24*, 3587.
(25) Green, P. F.; Kramer, E. J. *Macromolecules* **1986**, *19*, 1108.
(26) Tsenoglou, C. *J. Polym. Sci., Polym. Phys. Ed.* **1988**, *26*, 2329.
(27) Flory, P. J. *Statistical Mechanics of Chain Molecules*; Hanser: New York, 1989.
(28) Xu, Z.; Hadjichristidis, N.; Carella, J. M.; Fetters, L. J. *Macromolecules* **1983**, *16*, 925.
(29) Ronca, G. *J. Chem. Phys.* **1983**, *79*, 1031.
(30) Wu, S. *J. Polym. Sci., Polym. Phys. Ed.* **1989**, *27*, 723.
(31) Colby, R. H. *Polymer* **1989**, *30*, 1275.
(32) Zawada, J. A.; Ylitalo, C. M.; Fuller, G. G.; Colby, R. H.; Long, T. E. *Macromolecules* **1992**, *25*, 2896.
(33) Roovers, J.; Toporowski, P. M. *Macromolecules* **1991**, *25*, 1096.
(34) Brochard-Wyart, F. *C.R. Hebd. Seances Acad. Sci.* **1987**, *305*, 657.
(35) Composto, R. J.; Kramer, E. J.; White, D. M. *Polymer* **1990**, *31*, 2320.